



Universiteit
Leiden
The Netherlands

Supramolecular host-guest chemistry for applications in theranostics

Spa, S.J.

Citation

Spa, S. J. (2019, May 9). *Supramolecular host-guest chemistry for applications in theranostics*. Retrieved from <https://hdl.handle.net/1887/72514>

Version: Not Applicable (or Unknown)

License: [Leiden University Non-exclusive license](#)

Downloaded from: <https://hdl.handle.net/1887/72514>

Note: To cite this publication please use the final published version (if applicable).

Cover Page



Universiteit Leiden



The handle <http://hdl.handle.net/1887/72514> holds various files of this Leiden University dissertation.

Author: Spa, S.J.

Title: Supramolecular host-guest chemistry for applications in theranostics

Issue Date: 2019-05-09



CHAPTER **3**

**A Supramolecular Approach for
Liver Radioembolization**

ABSTRACT

Hepatic radioembolization therapies can suffer from discrepancies between diagnostic planning (scout-scan) and the therapeutic delivery itself, resulting in unwanted side-effects such as pulmonary shunting. We reasoned that a nanotechnology-based pre-targeting strategy could help overcome this shortcoming by directly linking pre-interventional diagnostics to the local delivery of therapy.

Methods

The host-guest interaction between adamantane and cyclodextrin was employed in an *in vivo* pre-targeting set-up. Adamantane (guest)-functionalized macro albumin aggregates (MAA-Ad; $d = 18 \mu\text{m}$) and (radiolabeled) Cy5 and β -cyclodextrin (host)-containing PIBMA polymers ($^{99\text{m}}\text{Tc-Cy5}_{0.5}\text{CD}_{10}\text{PIBMA}_{39}$; MW ~ 18.8 kDa) functioned as the reactive pair. Following liver or lung embolization with ($^{99\text{m}}\text{Tc}$)-MAA-Ad or ($^{99\text{m}}\text{Tc}$)-MAA (control), the utility of the pre-targeting concept was evaluated after intravenous administration of $^{99\text{m}}\text{Tc-Cy5}_{0.5}\text{CD}_{10}\text{PIBMA}_{39}$.

Results

Interactions between MAA-Ad and $\text{Cy5}_{0.5}\text{CD}_{10}\text{PIBMA}_{39}$ could be monitored in solution using confocal microscopy and were quantified by radioisotope-based binding experiments. *In vivo* the accumulation of the MAA-Ad particles in the liver or lungs yielded an approximate ten-fold increase in accumulation of $^{99\text{m}}\text{Tc-Cy5}_{0.5}\text{CD}_{10}\text{PIBMA}_{39}$ in these organs (16.2 %ID/g and 10.5 %ID/g, respectively) compared to the control. Pre-targeting with MAA alone was shown to be only half as efficient. Uniquely, for the first time, this data demonstrates that the formation of supramolecular interactions between cyclodextrin and adamantane can be used to drive complex formation in the chemically challenging *in vivo* environment.

Conclusion

The *in vivo* distribution pattern of the cyclodextrin host could be guided by the pre-administration of the adamantane guest, thereby creating a direct link between the scout-scan (MAA-Ad) and delivery of therapy.

INTRODUCTION

Radioembolization is a radiation-based therapeutic method that is applied for primary liver tumors and metastases that are untreatable via surgery or chemotherapy. During these interventions, microspheres that contain therapeutic radioisotopes (β -emitters such as yttrium-90 or holmium-166) are intrahepatically delivered.¹ While the clinical benefit of this approach has been demonstrated in large randomized controlled trials,²⁻⁴ the preclusion of hepatopulmonary shunting remains an unsolved challenge. Shunting results in the displacement of a fraction of the administered particles towards the microvasculature of the lung instead of the liver, leading to ineffective dose distribution and serious adverse effects such as radiation pneumonitis.⁵⁻⁷ To predict the likelihood of shunting prior to initiation of the therapeutic intervention, technetium-99m labelled macro albumin aggregates (^{99m}Tc-MAA; d = 18 μ m) can be administered as a diagnostic “scout” procedure. Besides insight into the degree of shunting, SPECT/CT-based ^{99m}Tc-MAA uptake monitoring also helps to provide a dosimetric (distribution) model for the therapeutic isotopes.^{6,8} Differences in particle composition and pharmacokinetics, however, do not fully exclude discrepancies between the “scout” procedure and the therapeutic delivery. As a result, hepatopulmonary shunting still occurs in over 13% of therapeutic interventions.⁹⁻¹¹ Unfortunately, when this occurs the implementation of preventive measures is no longer an option.

In an attempt to provide a more advanced theranostic solution for this problem, we investigated a two-step pre-targeting concept *in vivo*. The potential of an *in vivo* pre-targeting setup has been shown in radioimmunotherapy of cancer which has relied on, for example, the interactions between complementary oligonucleotides,¹² or bispecific- or avidin/biotinantibodies.¹³ However, this setup suffered from slow pharmacokinetics (at least 2 days between the first two injections), possible internalization of the antibody, and/or requires multiple (3-5) injection steps.¹³ To overcome these issues a different pre-targeting approach based on multivalent supramolecular host-guest interactions between adamantane (Ad) and β -cyclodextrin (CD; Figure 1A) was investigated. While CD has been utilized to form nanoparticles for drug delivery^{14,15} the host-guest chemistry was always performed beforehand, and not *in situ*. Recently, we successfully employed CD-Ad host-guest chemistry *in vitro*^{16,17} and, to the best of our knowledge, we now employ these chemical CD-Ad host-guest interactions *in vivo* for the first time.

Using Ad_x-guest-functionalized MAA microspheres (Figure 1A), the diagnostic MAA compound was converted into a pre-targeting vector for an intravenously (i.v.) administered

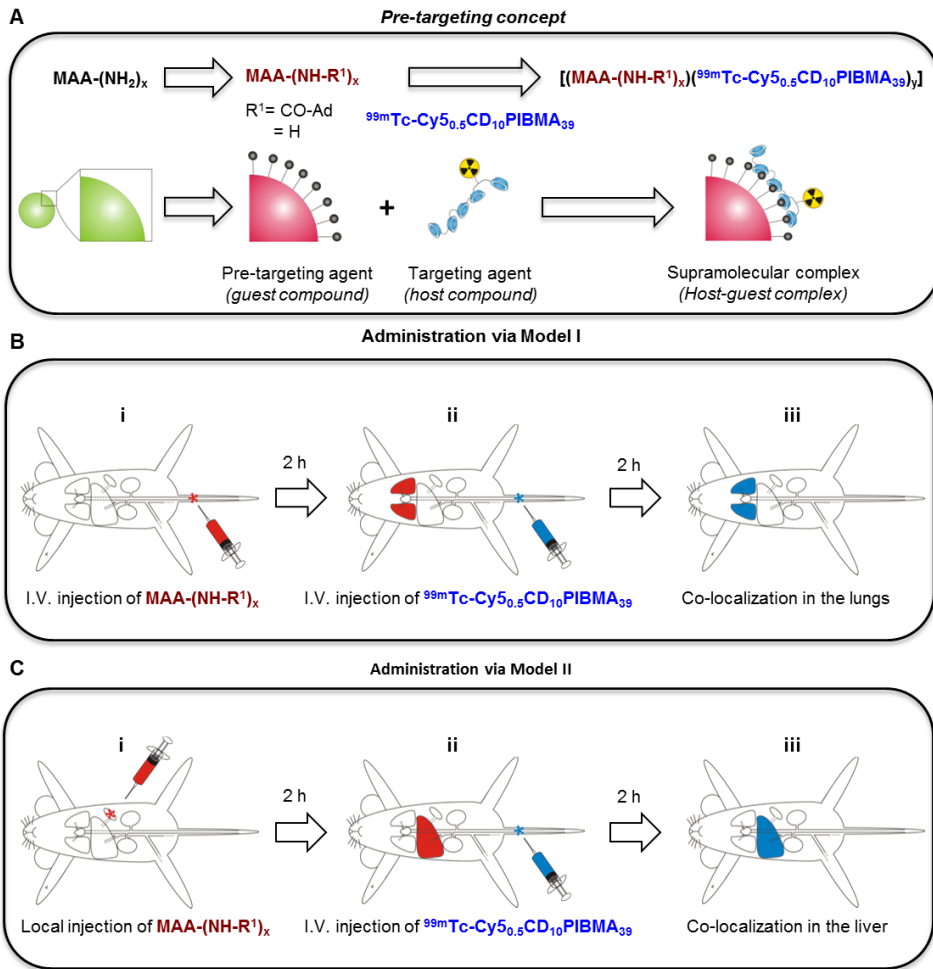


Figure 1. The radioembolization tailored pre-targeting concept is schematically illustrated by the chemical and functional steps involved. **A)** Representation of the different chemical functionalities and components. **B)** I.v. pre-administered MAA-Ad (Bi) accumulated in the lungs (Bii). Subsequent i.v. administration of $^{99m}Tc-Cy5_{0.5}CD_{10}PIBMA_{39}$ (Bii) resulted in pulmonary co-localization of MAA-Ad and $^{99m}Tc-Cy5_{0.5}CD_{10}PIBMA_{39}$ (Biii). **C)** Local pre-administered MAA-Ad (Ci) accumulated in the liver (Cii). Following i.v. administration of $^{99m}Tc-Cy5_{0.5}CD_{10}PIBMA_{39}$ (Cii) hepatic co-localization of both compounds was observed (Ciii).

radiolabeled β -cyclodextrin-PIBMA-polymer (host, Figure 1A). The β -cyclodextrin-polymer provides a platform for future functionalization with therapeutic radioisotopes. The pre-targeted radioembolization concept was tested via the use of two different pre-clinical

models that were either in line with: 1) the routine clinical use of ^{99m}Tc -MAA for lung staining, wherein MAA is administered intravenously (i.v.; Model I, Figure 1B), or 2) the current clinical set-up for locally administered hepatic radioembolization wherein MAA is administered locally (Model II, Figure 1C).

EXPERIMENTAL

General

For the stability of the compounds please see the Supplementary Material section. All chemicals were obtained from commercial sources and used without further purification. NMR spectra were obtained using a Bruker DPX 300 spectrometer (300 MHz, ^1H NMR) or a Bruker AVANCE III 500 MHz with a TXI gradient probe. All spectra were referenced to residual solvent signal or TMS. HPLC was performed on a Waters system using a 1525EF pump and a 2489 UV detector. For preparative HPLC, a Dr. Maisch GmbH, Reprosil-Pur 120 C18-AQ 10 μm column and a gradient of 0.1 % TFA in $\text{H}_2\text{O}/\text{CH}_3\text{CN}$ (95:5) to 0.1 % TFA in $\text{H}_2\text{O}/\text{CH}_3\text{CN}$ (5:95) in 40 min were used. For analytical HPLC, a Dr. Maisch GmbH, Reprosil-Pur C18-AQ 5 μm (250 \times 4.6 mm) column and a gradient of 0.1 % TFA in $\text{H}_2\text{O}/\text{CH}_3\text{CN}$ (95:5) to 0.1 % TFA in $\text{H}_2\text{O}/\text{CH}_3\text{CN}$ (5:95) in 40 min were used. MALDI-ToF measurements were performed on a Bruker Microflex. High-resolution mass spectra were measured on an Exactive orbitrap high-resolution mass spectrometer (Thermo Fisher Scientific, San Jose, CA) and processed with the use of Thermo Scientific Xcalibur software (V2.1.0.1139). For dialysis, Sigma Pur-ALyzerTM Mega 3,500 units were used.

Synthesis

Adamantane-tetrafluorophenol (Ad-TFP)

1-Adamantanecarboxylic acid (500 mg, 2.8 mmol) and 2,3,5,6-tetrafluorophenol (TFP) (718 mg, 4.3 mmol) were dissolved in 10 mL dry dichloromethane (DCM) and stirred for 10 min. Subsequently, *N,N*-dicyclohexylcarbodiimide (858 mg, 4.3 mmol), dissolved in 5 mL dry DCM, was added drop-wise. After stirring for 2 days at RT, the reaction mixture was filtered and the filtrate was concentrated in vacuo. The resulting yellow product was purified by silica column chromatography (DCM:Hexane, 1:1). Pure fractions were pulled and concentrated under vacuum to obtain the product as a white crystalline powder (785 mg, 86%). ^1H NMR (300 MHz, CDCl_3 , 25 $^\circ\text{C}$) = δ 7.06 – 6.89 (m, 1H, CH of TFP), 2.09 (s, 9H, C-CH₂-CH and CH₂-CH-CH₂), 1.78 (s, 6H, CH-CH₂-CH). High resolution mass: $[\text{C}_{17}\text{H}_{17}\text{F}_4\text{O}_2]^+$ calculated 329.3, found 328.1 (Figure S1).

Cy5-(SO₃)Sulfonate-(SO₃)COTFP

Cy5-(SO₃)Sulfonate-(SO₃)COOH was synthesized according to an earlier published procedure.¹⁸

Cy5_{0.5}CD₁₀PIBMA₃₉

The synthesis of Cy5_{0.5}CD₁₀PIBMA₃₉ was performed according to a recently described procedure.¹⁶

Functionalization of macro-aggregates with adamantane (MAA-Ad)

Albumin macro-aggregates (TechneScan®, MAA) were obtained from Mallinckrodt Medical B.V., Petten, The Netherlands. Lyophilized macroaggregates (2 mg) were dissolved in 1 mL of saline (0.9% NaCl, sterile and pyrogen-free, B. Braun Medical Supplies, Inc., Oss, The Netherlands) and portions of 0.1 mL (containing 0.2 mg MAA) were stored in Eppendorf tubes at -20 °C until further use. For functionalization, one portion was defrosted and 20 µL of Ad-TFP (10 mg/mL DMSO) was added. After agitation in a shaking water bath for 1 h at 37 °C, the solution was washed 2 times with phosphate buffered saline (PBS) by 2 centrifugation steps (3 min, 3000 ×g). The obtained MAA-Ad was diluted in 1 mL of PBS to 0.2 mg/mL.

To estimate the number of Ad conjugated to MAA, the MAA functionalization was also performed with Cy5-TFP according to the same procedure as for Ad-TFP. Subsequently, the absorbance at 650 nM of the MAA-Cy5 constructs was measured using a NanoDrop Spectrophotometer (Thermo Fisher Scientific Inc. Wilmington, DE, USA). The dye concentration was calculated using the absorbance following the law of Lambert Beer ($A = \epsilon \cdot l \cdot C$) with $\epsilon_{\text{Cy5}} = 250 \times 10^3 \text{ mol}^{-1}\text{cm}^{-1}$. The number of Cy5/MAA aggregates was then calculated by dividing the calculated Cy5 concentration by the known MAA concentration, resulting in a ratio of $3.07(\pm 0.24) \times 10^8$ Cy5/MAA particle on average. Assuming that Ad-TFP reacts in a similar fashion as Cy5-TFP, it was estimated that the ratio of Ad/MAA would be of the same order of magnitude.

Radiolabeling of Cy5_{0.5}CD₁₀PIBMA₃₉

Radiolabeling of Cy5_{0.5}CD₁₀PIBMA₃₉ was performed as follows: to 10 mL of Cy5_{0.5}CD₁₀PIBMA₃₉ (1 mg/mL in PBS), 4 mL of SnCl₂·2H₂O (0.44 mg/mL saline, Technescan PYP, Mallinckrodt Medical B.V.), and 100 mL of a freshly eluted ^{99m}Tc-Na-pertechnetate solution (500 MBq/mL, Mallinckrodt Medical B.V.) were added, and the mixture was gently stirred in a shaking water bath for 1 h at 37 °C.¹⁹ Subsequently, the labeling yield

was estimated over time by ITLC analysis according to the following procedure: 2 mL of the reaction mixture was applied on 1x7 cm ITLC-SG paper strips (Agilent Technologies, USA) for 10 min at RT with PBS as the mobile phase. After 1 h, the highest labeling yield of Cy5_{0.5}CD₁₀PIBMA₃₉ with ^{99m}Tc was assessed (49.6%) and the reaction mixture was purified by size exclusion chromatography with sterile PBS as the mobile phase using Sephadex™ G-25 (desalting columns PD-10, GE Healthcare Europe GmbH, Freiburg, Germany). Fractions containing ^{99m}Tc-Cy5_{0.5}CD₁₀PIBMA₃₉ were collected and directly applied in the imaging experiments.

Radiostability in PBS

To assess the stability of the radiolabeling in PBS, after 24 h the release of radioactivity from PD-10-purified ^{99m}Tc-Cy5_{0.5}CD₁₀PIBMA₃₉ was determined with ITLC (according to the same method described in 'Radiolabeling of Cy5_{0.5}CD₁₀PIBMA₃₉').

Supramolecular interaction between MAA-Ad and ^{99m}Tc-Cy5_{0.5}CD₁₀PIBMA₃₉

To determine the supramolecular interaction between MAA-Ad and Cy5_{0.5}CD₁₀PIBMA₃₉ *in vitro*, 0.1 mL of MAA-Ad in PBS (0.2 mg/mL) and 0.1 mL of ^{99m}Tc-Cy5_{0.5}CD₁₀PIBMA₃₉ in PBS (1 mg/mL, 1 MBq) were mixed and the solution was incubated for 1 h in a shaking water bath at 37 °C. Thereafter, the radioactivity of the total amount added and the radioactivity of the pellet after two washing steps with PBS were measured in a dose-calibrator to determine the amount of binding of ^{99m}Tc-Cy5_{0.5}CD₁₀PIBMA₃₉ to MAA-Ad. After correction for background activity, the amount of binding was expressed as the percentage of the total amount of radioactivity (%binding). To assess the effect of the Ad moieties, the same experiment was also performed with non-functionalized MAA and the resulting %binding of ^{99m}Tc-Cy5_{0.5}CD₁₀PIBMA₃₉ to MAA and MAA-Ad were compared (Figure 2B). Significance between the two conditions was calculated using a two-tailed student's t-Test with n = 4.

The supramolecular interaction between MAA-Ad and Cy5_{0.5}CD₁₀PIBMA₃₉ was also visualized by confocal microscopy, employing the Cy5 component of the polymer.¹⁶ For this purpose, the same experiment was repeated, but this time non-radioactive Cy5_{0.5}CD₁₀PIBMA₃₉ was added to the MAA and MAA-Ad solutions. After washing, 10 mL of MAA (with or without-Ad) Cy5_{0.5}CD₁₀PIBMA₃₉ solution was pipetted onto culture dishes with glass inserts (ø35mm glass bottom dishes No. 15, poly-d-lysine coated, γ-irradiated, MatTek corporation). Images were taken on a Leica SP5 WLL confocal microscope under 63x magnification using Leica Application Suite software. Cy5 fluorescence was measured with excitation at 633 nm and emission was collected at 650-700 nm.

In vivo studies

Animals

All *in vivo* studies were performed using 10-12 week old Swiss mice (20-25 g, Crl:OF1 strain, Charles River Laboratories, USA). All animal studies were approved by the institutional Animal Ethics Committee (DEC permit 12160) of the Leiden University Medical Center. All mice were kept under specific pathogen-free conditions in the animal housing facility of the LUMC. Food and water were given *ad libitum*.

General SPECT imaging and biodistribution protocol

SPECT imaging was performed at 2 h after injection of ^{99m}Tc-labeled compounds. Mice were placed onto a dedicated positioning bed of a three-headed U-SPECT-2 (MILabs, Utrecht, the Netherlands) under continuous 1-2% isoflurane anesthesia.²⁰ Radioactivity counts from total body scans or selected regions of interest (ROI) were acquired for 60 min using a 0.6 mm mouse multi-pinhole collimator in list mode data. For reconstruction from list mode data, the photo peak energy window was centered at 140 keV with a window width of 20%. Side windows of 5% were applied to correct for scatter and down scatter corrections. The image was reconstructed using 24 Pixel based Ordered Subset Expectation Maximization iterations (POSEM) with 4 subsets, 0.2 mm isotropic voxel size and with decay and triple energy scatter correction integrated into the reconstruction with a post filter setting of 0.25 mm.²¹ Volume rendered images were generated from 2-4 mm slices and analyzed using Matlab R2014a software (version 8.3.0.532, MathWorks® Natick, MA). Images were generated from maximum intensity protocols (MIP) adjusting the color scale threshold to optimal depiction of the tissues of interest.²² After imaging, the mice were euthanized by an intraperitoneal injection of 0.25 mL Euthasol (ASTfarma, Oudewater, The Netherlands).

To determine the biodistribution of the tracer, organs were collected from mice and counted for radioactivity in a dose-calibrator (VDC 101, Veenstra Instruments, Joure, the Netherlands) or a gamma counter (Wizard2 2470 automatic gamma scintillation counter, Perkin Elmer). After collecting and counting all tissues together with the remaining activity in the carcass, the total amount of remaining radioactivity in the animal was counted and, after correction for physical decay, the urinary excretion expressed as the percentage of the total injected dose (%ID) was calculated. Radioactivity counts in tissues were expressed as the percentage of the total injected dose of radioactivity per gram tissue (%ID/g). Additionally, reconstructed images were generated and analyzed using Amide 1.0.2 software (<http://amide.sourceforge.net/documentation.html>).²³

Mapping the distribution of $^{99m}\text{Tc-Cy5}_{0.5}\text{CD}_{10}\text{PIBMA}_{39}$ in mice

To determine the natural distribution of $^{99m}\text{Tc-Cy5}_{0.5}\text{CD}_{10}\text{PIBMA}_{39}$, 0.1 mL of PBS containing $^{99m}\text{Tc-Cy5}_{0.5}\text{CD}_{10}\text{PIBMA}_{39}$ (1 mg/mL, 20 MBq) was injected i.v. 2 h after injection, SPECT imaging and biodistribution studies were performed as described above (Figure 3A, D).

Mapping the distribution of ^{99m}Tc -labeled MAA-Ad in mice via:

i.v. administration, Model I

To determine whether MAA embolizations are tolerated by mice and whether MAA-Ad is delivered to the capillaries of the lungs, MAA-Ad was radiolabeled according to the manufacturer's instructions, and 0.1 mL of $^{99m}\text{Tc-MAA-Ad}$ in PBS (0.02 mg, 2 mg/mL) was injected into the tail vein. At 2 h after injection, the organ distribution of the tracer in mice was imaged using SPECT and quantified with biodistribution studies (see SPECT imaging protocol and biodistribution studies described above (Figure 3 B, D).

Local administration, model II

An embolization setup in the liver was performed to mimic the clinical setup for liver radioembolization.²⁴ For this purpose, animals were anesthetized by intraperitoneal injection of a mixture containing Hypnorm (Vetapharma, Leeds, United Kingdom), dormicum (Roche, Basel, Switzerland), and water (1:1:2). After shaving and cleaning with ethanol (70%), the abdominal cavity was incised for 0.5 cm and the spleen was exposed outside the mouse. Of the $^{99m}\text{Tc-MAA-Ad}$ solution (2 mg/mL), 100 μL was injected into the spleen using a Myjector U-100 insulin syringe (29G x $\frac{1}{2}$ " 0.33 x12 mm, Terumo Europe, Leuven, Belgium) and after 5 s the needle was removed and the spleen was positioned inside the peritoneal cavity. The incision was sutured by 2-4 stitches and the animals were placed under a heating lamp to maintain the body temperature at 37 °C. At 2 h after injection, the organ distribution of the tracer in mice was imaged using SPECT and quantitated with biodistribution studies as described above (Figure 3C, D).

Mapping the distribution of $^{99m}\text{Tc-Cy5}_{0.5}\text{CD}_{10}\text{PIBMA}_{39}$ after MAA(-Ad) pre-administration

The influence of MAA or MAA-Ad on the distribution of $^{99m}\text{Tc-Cy5}_{0.5}\text{CD}_{10}\text{PIBMA}_{39}$ was evaluated as follows: first, 0.1 mL containing MAA-Ad or non-functionalized MAA in 0.1 mL (0.02 mg, 2 mg/mL) was injected by either i.v. administration (Figure 1B, Model I) or local administration (Figure 1C, Model II). After 2 h, 0.1 mL of $^{99m}\text{Tc-Cy5}_{0.5}\text{CD}_{10}\text{PIBMA}_{39}$ in PBS (1 mg/mL, 20 MBq) was i.v. injected and another 2 h later SPECT imaging and biodistribution studies were performed as described above (Figure 4).

RESULTS AND DISCUSSION

To allow for initial diagnostics of the particle distribution and to provide a guest-particle that can act as an *in vivo* target, clinical grade MAA particles were functionalized with Ad guest moieties (Figure 1A) via amide bond formation. This yielded MAA-Ad with, on average, 10^8 Ad molecules per MAA particle. Especially for these experiments a fluorescent β -cyclodextrin-poly(isobutylene-alt-maleic-anhydride)-polymer host molecule (Cy5_{0.5}CD₁₀PIBMA₃₉, ~18.8 kDa, diameter, ~11.7 nm) was synthesized (Figure 1A),¹⁶ that contained (on average) ten β -CD compounds. Besides CD, various carboxylic acid groups were present on the backbone of the polymer that could serve as the chelating ligand for a range of metal ion-based radio-isotopes, such as ⁹⁰Y, ¹⁶⁶Ho, and ^{99m}Tc.

The interaction between CD and Ad is well-known, with a binding affinity of $\sim 5 \times 10^4$ M⁻¹ for a monovalent interaction.²⁵ Increasing the number of host and guest moieties drives multivalent interactions, which effectively increases the binding affinity.²⁶ Evidence that individual compounds effectively form complexes based on intended Ad-CD binding interactions was demonstrated *in vitro*. While MAA alone did induce some Cy5_{0.5}CD₁₀PIBMA₃₉ accumulation, clearly a higher level of Cy5_{0.5}CD₁₀PIBMA₃₉ accumulation was obtained with MAA-Ad (Figure 2A). The difference in accumulation was quantified by a radioisotope-based binding experiment with ^{99m}Tc-Cy5_{0.5}CD₁₀PIBMA₃₉. This experiment revealed a significant ($p < 0.01$) 5.7-fold increase (Figure 2B) in ^{99m}Tc-Cy5_{0.5}CD₁₀PIBMA₃₉ accumulation with MAA-Ad (49.2%) versus MAA (8.6%), underlining that the observed complex formation is indeed facilitated by the intended Ad-CD host-guest interactions.

To create a reference for the *in vivo* binding between Cy5_{0.5}CD₁₀PIBMA₃₉ and MAA-Ad, first the biodistribution of *i.v.* administered ^{99m}Tc-Cy5_{0.5}CD₁₀PIBMA₃₉ was studied without any pre-targeting vector present. This yielded a low overall organ uptake (~ 1.5 %ID/g, Figure 3A, D). Secondly, the distribution of the pre-targeting vector ^{99m}Tc-MAA-Ad in both the *i.v.* and local administration model was determined. SPECT imaging and biodistribution studies at 2 h post tracer administration revealed a distinct distribution pattern of ^{99m}Tc-MAA-Ad for Model I (*i.v.*) and Model II (local, Figure 3A, 3B). In agreement with previous reports on the distribution of ^{99m}Tc-MAA after *i.v.* injection,²⁷ Model I showed high levels of accumulation of ^{99m}Tc-MAA-Ad in the lungs (335 %ID/g). Local administration of ^{99m}Tc-MAA-Ad, whereby hepatic tracer delivery was realized through injection into parenchymal tissue of the spleen (Model II),²⁸ resulted in high uptake levels in the liver (50.4 %ID/g).

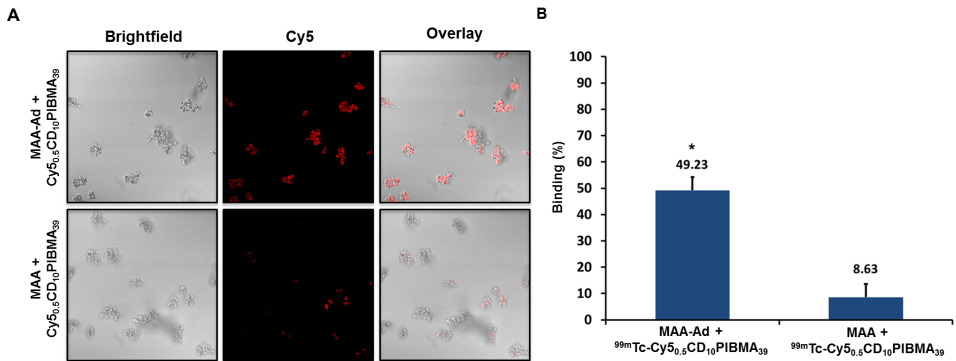


Figure 2. **A**) Fluorescence confocal microscopy-based evaluation of Cy5_{0.5}CD₁₀PIBMA₃₉ (Cy5) binding to MAA-Ad (top) and non-functionalized MAA (bottom). The MAA-Ad localized particles (brightfield) reveal a higher degree of staining compared to MAA alone, indicated by the higher Cy5-related fluorescence intensities (in red). **B**) The binding of ^{99m}Tc-Cy5_{0.5}CD₁₀PIBMA₃₉ to MAA-Ad and MAA quantified by radioactivity and expressed as a percentage of the total amount of radioactivity (^{99m}Tc-Cy5_{0.5}CD₁₀PIBMA₃₉) added. Showing 5.7 times more binding to MAA functionalized with the Ad guest moiety compared to non-functionalized MAA, with a significance of difference of P < 0.01.

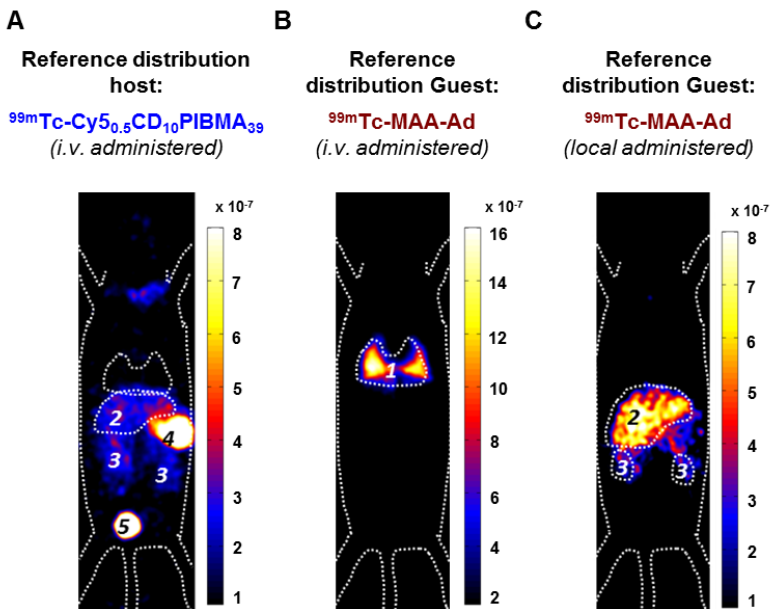


Figure 3. Reference SPECT and biodistribution data of i.v.-administered ^{99m}Tc-Cy5_{0.5}CD₁₀PIBMA₃₉ and i.v.- or locally administered ^{99m}Tc-MAA-Ad. **A**) Following i.v. administration of the targeted (host) agent ^{99m}Tc-Cy5_{0.5}CD₁₀PIBMA₃₉ no prominent distribution to the kidneys, liver or lungs was observed. **B** and **C**) The pre-targeting (guest) agent ^{99m}Tc-MAA-Ad displayed either pulmonary (B) or hepatic (C) accumulation depending on the route of administration (i.v. or local). Organs are marked as (1) lungs, (2) liver, (3) kidneys, (4) stomach, and (5) urinary bladder.

Table 1. Reference biodistributions of i.v.-administered $^{99m}\text{Tc-Cy5}_{0.5}\text{CD}_{10}\text{PIBMA}_{39}$ and i.v.- or locally administered $^{99m}\text{Tc-MAA-Ad}$. Data (expressed as the mean of the percentage of the injected dose per gram tissue (%ID/g) of 5 observations) were calculated based on the radioactive counts measured in various tissues at 2 h post-injection of the radioactive tracer.

Tissue	Reference distribution host	Reference distribution guest	
	$^{99m}\text{Tc-Cy5}_{0.5}\text{CD}_{10}\text{PIBMA}$ mean	Model I: $^{99m}\text{Tc-MAA-Ad}$ mean	Model II: $^{99m}\text{Tc-MAA-Ad}$ mean
Blood	2.4 ± 1.3	2.7 ± 0.9	1.0 ± 0.6
Lungs	1.7 ± 0.5	335.8 ± 38.7	4.4 ± 1.2
Spleen	0.9 ± 0.4	0.9 ± 0.2	6.1 ± 2.4
Liver	1.0 ± 0.2	1.3 ± 0.4	50.4 ± 15.4
Kidneys	4.7 ± 1.3	1.8 ± 0.6	15.3 ± 2.7
Muscle	0.4 ± 0.2	0.3 ± 0.1	0.9 ± 0.3
Brain	0.1 ± 0.0	0.1 ± 0.1	0.2 ± 0.1

The influence of local MAA(-Ad) deposits on the distribution of i.v.-administered $^{99m}\text{Tc-Cy5}_{0.5}\text{CD}_{10}\text{PIBMA}_{39}$ was studied via Model I (Figure 1B). Here the biodistribution of $^{99m}\text{Tc-Cy5}_{0.5}\text{CD}_{10}\text{PIBMA}_{39}$ after i.v. pre-administration of MAA and MAA-Ad (Figure 4A, B) was compared with the reference distribution of $^{99m}\text{Tc-Cy5}_{0.5}\text{CD}_{10}\text{PIBMA}_{39}$ (no MAA(-Ad) administered, Figure 3A, S2). Pre-targeting with non-functionalized MAA did not lead to changes in the distribution of $^{99m}\text{Tc-Cy5}_{0.5}\text{CD}_{10}\text{PIBMA}_{39}$ (Figure 4A, S2). More specifically, uptake levels in both the lungs and liver remained around 1.5 %ID/g (Figure 4E, 5A). Pre-targeting with MAA-Ad, however, did induce clear alterations in the distribution pattern of $^{99m}\text{Tc-Cy5}_{0.5}\text{CD}_{10}\text{PIBMA}_{39}$ (Figure 4B) as uptake in the lungs increased 6.2-fold (10.5 %ID/g, Figure 4E, 5A). Interestingly, the uptake in the liver also increased towards 5.7 %ID/g, while both the i.v. administration of $^{99m}\text{Tc-MAA-Ad}$ and $^{99m}\text{Tc-Cy5}_{0.5}\text{CD}_{10}\text{PIBMA}_{39}$ alone did not lead to significant liver uptake. It appears that the presence of $^{99m}\text{Tc-Cy5}_{0.5}\text{CD}_{10}\text{PIBMA}_{39}$ influenced the retention of MAA-Ad, causing partial displacement of the (complexed) compounds towards the liver. Alternatively, Ad-labeled metabolites of MAA-Ad could have migrated to the liver, thereby providing a platform for $^{99m}\text{Tc-Cy5}_{0.5}\text{CD}_{10}\text{PIBMA}_{39}$ binding.

To assess the value of pre-targeting in the liver, which is representative of the clinical radioembolization procedure, the same host-guest setup was applied following intrahepatic deposition (Model II; Figure 1C). In this model, the influence of MAA-Ad was even more profound. The presence of low quantities of uptake in the salivary glands and the stomach (Table S1, Figure S2) is indicative for the presence of some free ^{99m}Tc (see Supplementary Material for further stability details).²⁹ Compared to the control, pre-targeting with non-

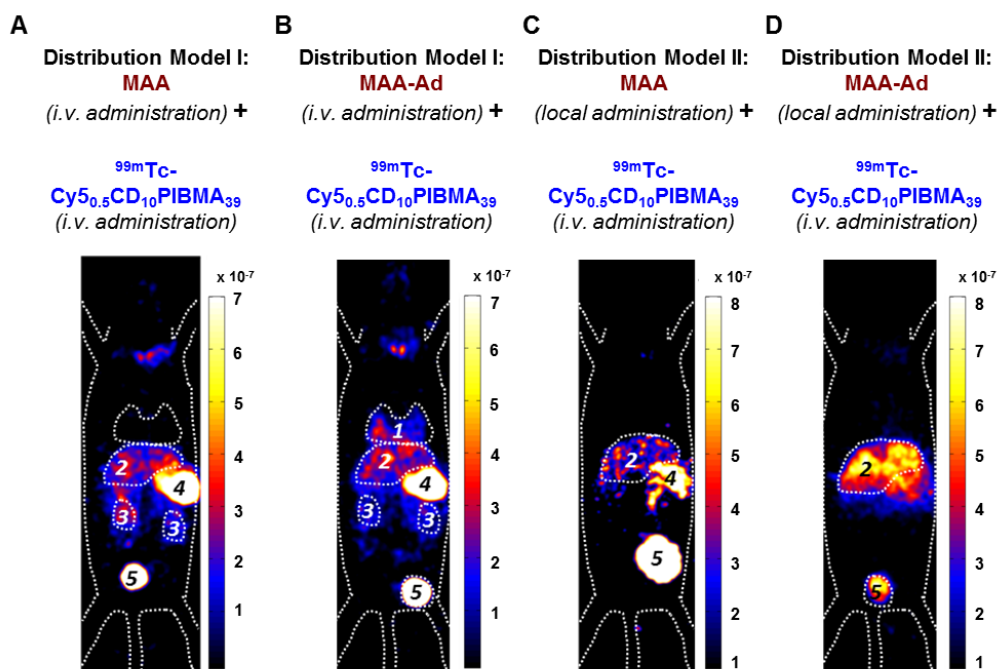


Figure 4. SPECT and biodistribution data of i.v.-administered $^{99m}\text{Tc-Cy5}_{0.5}\text{CD}_{10}\text{PIBMA}_{39}$ after pre-targeting with MAA or MAA-Ad either i.v. (Model I) or locally (Model II) administered. **A)** Following i.v. administration of MAA, no pulmonary accumulation of $^{99m}\text{Tc-Cy5}_{0.5}\text{CD}_{10}\text{PIBMA}_{39}$ was observed. **B)** i.v. pre-administered Ad-functionalized MAA did lead to pulmonary accumulation of $^{99m}\text{Tc-Cy5}_{0.5}\text{CD}_{10}\text{PIBMA}_{39}$. **C)** Following local administration of MAA, slight uptake in liver and kidneys occurred. **D)** After pre-targeting with MAA-Ad, the hepatic accumulation of $^{99m}\text{Tc-Cy5}_{0.5}\text{CD}_{10}\text{PIBMA}_{39}$ was even more profound. Organs are marked as (1) lungs, (2) liver, (3) kidneys, (4) stomach, and (5) urinary bladder.

functionalized MAA resulted in increased uptake levels of $^{99m}\text{Tc-Cy5}_{0.5}\text{CD}_{10}\text{PIBMA}_{39}$ in the liver (8.7 %ID/g) and kidneys (10.7 %ID/g), but not in the lungs (1.4 %ID/g, Table 1 vs. Figure 4C, Table 2). This complex formation is in line with that observed during the radioisotope-based in vitro binding experiments in solution (Figure 2). After pre-targeting with MAA-Ad, the differences became more distinct, yielding a 15.7-fold increase in liver uptake (16.2 %ID/g) and a 4.5-fold increase in kidney uptake (19.6 %ID/g) (Figure 4D, E, 5B). Both uptake profiles are in accordance with the distribution pattern of locally administered $^{99m}\text{Tc-MAA-Ad}$ (Figure 3C). As was concluded from the in situ binding, the liver uptake induced by MAA-Ad was nearly double that observed using MAA only. Clearly the host-guest complex formation is more efficient in the liver than in the lungs (see Figure 5). This is likely to be related to the 1,000-fold reduction in particle velocity experienced as they traverse the

Table 2. Biodistribution of $^{99m}\text{Tc-Cy5}_{0.5}\text{CD}_{10}\text{PIBMA}_{39}$ after pre-targeting with i.v.- (Model I) or locally (Model II) administered MAA or MAA-Ad. Data (expressed as the mean of the percentage of the injected dose per gram tissue (%ID/g) of 5 observations) were calculated based on the radioactive counts measured in various tissues at 2 h post-injection of the radioactive tracer.

Distribution of host ($^{99m}\text{Tc-Cy5}_{0.5}\text{CD}_{10}\text{PIBMA}_{39}$) following injection of indicated guest				
Tissue	Model I: MAA Mean	Model I: MAA-Ad Mean	Model II: MAA Mean	Model II: MAA-Ad mean
Blood	2.1 ± 1.0	1.9 ± 0.5	1.9 ± 0.3	3.8 ± 0.6
Lungs	1.6 ± 0.7	10.5 ± 4.6	1.4 ± 0.7	2.6 ± 0.2
Spleen	1.2 ± 0.4	4.7 ± 2.3	4.7 ± 1.3	10.4 ± 1.4
Liver	2.2 ± 0.9	5.7 ± 0.9	8.7 ± 1.0	16.2 ± 0.7
Kidneys	4.1 ± 1.7	6.6 ± 2.0	10.7 ± 0.8	19.6 ± 3.8
Muscle	0.5 ± 0.2	0.5 ± 0.2	0.5 ± 0.1	0.8 ± 0.4
Brain	0.3 ± 0.4	0.2 ± 0.2	0.1 ± 0.1	0.1 ± 0.0

vasculature of the liver, a feature that was said to result in 7.5-times higher interaction rates between particles and hepatic cells.³⁰ The flow reduction may also be enhanced further following partial blockage (embolization) of capillary vessels by MAA(-Ad).

Taken together, the combined distribution data for Model I and Model II clearly indicate that the *in vivo* distribution pattern of the multimeric $^{99m}\text{Tc-Cy5}_{0.5}\text{CD}_{10}\text{PIBMA}_{39}$ host molecule, which served as a model for a future therapeutic agent, can be guided by a pre-targeting approach that makes use of Ad-functionalized microspheres. The fact that the supramolecular interactions in the liver are stronger than those in the lungs indicates that in this pre-targeting model, pulmonary shunting during liver embolization procedures would only result in limited unwanted side-effects. Furthermore, although not yet explored in this study, in the future the polymer-based building blocks can be synthetically modified to: i) optimize their pharmacokinetics and ii) act as carriers for other (therapeutic) isotopes or drugs, e.g., for chemo-embolization.^{29,31,32} Alternatively, local (e.g. intratumoral) deposits of albumin-based particles could not only be used to mark tumors for surgical resection.³³ In a pre-targeting approach such particles could also help provide local therapy.

In previous studies we have demonstrated that supramolecular chemistry can be used to generate clinical grade imaging agents, such as indocyanine green (ICG)- ^{99m}Tc -nanocolloid.^{31,32} This multimodal nanoparticle has helped to connect pre- and intraoperative imaging, and as such, realized image-guided surgery of infected lymph nodes. In the present study, we successfully applied a different supramolecular interaction *in vivo* to advance a theranostic medical intervention, namely radioembolization.

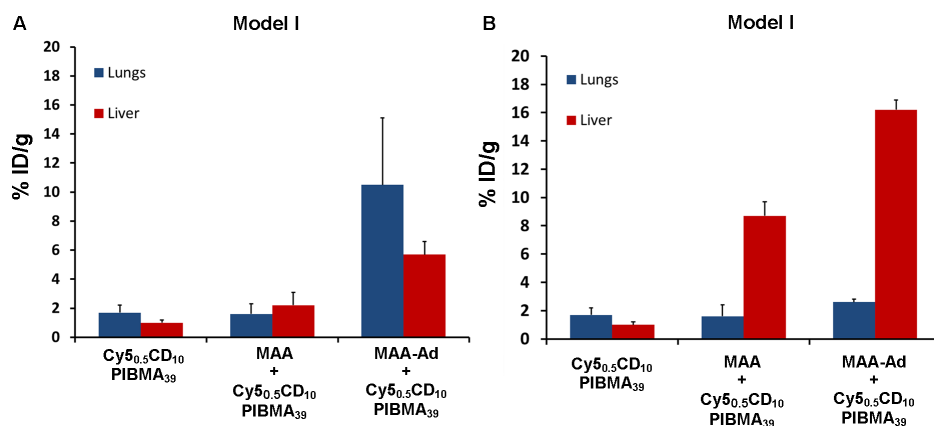


Figure 5. Influence of MAA(-Ad) on the uptake of $^{99m}\text{Tc-Cy}_{5.0.5}\text{CD}_{10}\text{-PIBMA}_{39}$ in the lungs and liver (Table 1 and 2). **A)** Uptake in the lungs increased when MAA-Ad was administered i.v. (Method I). **B)** Increasing uptake in the liver was seen when MAA-Ad was administered locally (Method II). The significance of difference ($P < 0.01$) is indicated with *

CONCLUSION

The initial proof-of-concept data presented demonstrates that despite the chemically complex in vivo environment, multivalent host-guest interactions between Ad and CD can still be formed. Depending on the route of MAA-Ad administration (i.v. or local), the degree and location of $^{99m}\text{Tc-Cy}_{5.0.5}\text{CD}_{10}\text{-PIBMA}_{39}$ accumulation could be guided. For future radioembolization applications this would mean that the distributions observed in the scout scan would directly correlate to those of the therapeutic radioisotope delivery (e.g., ^{90}Y or ^{166}Ho). Overall, a versatile new chemical platform for translational theranostic pre-targeting has been generated.

Acknowledgements

The research leading to these results was funded with grants from: the European Research Council (ERC) under the European Union's Seventh Framework Program FP7/2007-2013 (grant agreement number 2012-306890), from the Netherlands Organization for Scientific Research (NWO nano-Grant STW 11435 and VIDI-grant - STW BGT11272) and the 2015-2016 Postdoctoral Molecular Imaging Scholar Program Grant granted by the Society of Nuclear Medicine and Molecular Imaging (SNMMI) and the Education and Research Foundation (ERF) for Nuclear Medicine and Molecular Imaging. We acknowledge Mark T. M. Rood for providing $\text{Cy}_{5.0.5}\text{CD}_{10}\text{-PIBMA}_{39}$.

REFERENCES

1. R. Hickey; R. J. Lewandowski; T. Prudhomme, et al., 90Y Radioembolization of Colorectal Hepatic Metastases Using Glass Microspheres: Safety and Survival Outcomes from a 531-Patient Multicenter Study. *Journal of nuclear medicine : official publication, Society of Nuclear Medicine* **2016**, 57 (5), 665-71.
2. P. Hilgard; M. Hamami; A. E. Fouly, et al., Radioembolization with yttrium-90 glass microspheres in hepatocellular carcinoma: European experience on safety and long-term survival. *Hepatology* **2010**, 52 (5), 1741-9.
3. A. Kennedy; D. Coldwell; B. Sangro, et al., Radioembolization for the treatment of liver tumors general principles. *American journal of clinical oncology* **2012**, 35 (1), 91-9.
4. C. E. Rosenbaum; H. M. Verkooijen; M. G. Lam, et al., Radioembolization for treatment of salvage patients with colorectal cancer liver metastases: a systematic review. *Journal of nuclear medicine : official publication, Society of Nuclear Medicine* **2013**, 54 (11), 1890-5.
5. M. Cremonesi; C. Chiesa; L. Strigari, et al., Radioembolization of hepatic lesions from a radiobiology and dosimetric perspective. *Frontiers in oncology* **2014**, 4, 210.
6. A. J. A. T. Braat; M. L. J. Smits; M. N. G. J. A. Braat, et al., 90Y Hepatic Radioembolization: An Update on Current Practice and Recent Developments. *J. Nucl. Med.* **2015**, 56 (7), 1079-1087.
7. A. F. van den Hoven; C. E. Rosenbaum; S. G. Elias, et al., Insights into the Dose-Response Relationship of Radioembolization with Resin 90Y-Microspheres: A Prospective Cohort Study in Patients with Colorectal Cancer Liver Metastases. *Journal of nuclear medicine : official publication, Society of Nuclear Medicine* **2016**, 57 (7), 1014-9.
8. S. Shanehsazzadeh; A. Lahooti; H. Yousefnia, et al., Comparison of estimated human dose of (68)Ga-MAA with (99m)Tc-MAA based on rat data. *Annals of nuclear medicine* **2015**, 29 (8), 745-53.
9. E. Garin; Y. Rolland; S. Laffont, et al., Clinical impact of (99m)Tc-MAA SPECT/CT-based dosimetry in the radioembolization of liver malignancies with (90)Y-loaded microspheres. *European journal of nuclear medicine and molecular imaging* **2016**, 43 (3), 559-75.
10. T. W. Leung; W. Y. Lau; S. K. Ho, et al., Radiation pneumonitis after selective internal radiation treatment with intraarterial 90yttrium-microspheres for inoperable hepatic tumors. *Int. J. Radiat. Oncol. Biol. Phys.* **1995**, 33 (4), 919-24.
11. A. K. Jha; N. Purandare; S. A. Shah, et al., Is there a correlation between planar scintigraphy after Tc-99m-MAA and Y-90 administration? *Nucl. Med. Commun.* **2016**, 37 (2), 107-109.

12. M. Patra; K. Zarschler; H. J. Pietzsch, et al., New insights into the pretargeting approach to image and treat tumours. *Chemical Society reviews* **2016**, *45* (23), 6415-6431.
13. O. C. Boerman; F. G. van Schaijk; W. J. G. Oyen, et al., Pretargeted Radioimmunotherapy of Cancer: Progress Step by Step. *Journal of nuclear medicine : official publication, Society of Nuclear Medicine* **2003**, *44*, 400-411.
14. S. Gaur; Y. Wang; L. Kretzner, et al., Pharmacodynamic and pharmacogenomic study of the nanoparticle conjugate of camptothecin CRLX101 for the treatment of cancer. *Nanomedicine : nanotechnology, biology, and medicine* **2014**, *10* (7), 1477-86.
15. Z. Dan; H. Cao; X. He, et al., Biological stimuli-responsive cyclodextrin-based host-guest nanosystems for cancer therapy. *International journal of pharmaceutics* **2015**, *483* (1-2), 63-8.
16. M. T. Rood; S. J. Spa; M. M. Welling, et al., Obtaining control of cell surface functionalizations via Pre-targeting and Supramolecular host guest interactions. *Scientific reports* **2017**, *7*, 39908.
17. M. Oikonomou; J. Wang; R. R. Carvalho, et al., Ternary supramolecular quantum-dot network flocculation for selective lectin detection. *Nano Res* **2016**, *9* (7), 1904-1912.
18. S. J. Spa; A. Bunschoten; M. T. M. Rood, et al., Orthogonal Functionalization of Ferritin via Supramolecular Re-Assembly. *Eur J Inorg Chem* **2015**, *2015* (27), 4603-4610.
19. M. M. Welling; A. Paulusma-Annema; H. S. Balter, et al., Technetium-99m labelled antimicrobial peptides discriminate between bacterial infections and sterile inflammations. *European journal of nuclear medicine* **2000**, *27* (3), 292-301.
20. M. M. Welling; A. Bunschoten; J. Kuil, et al., Development of a Hybrid Tracer for SPECT and Optical Imaging of Bacterial Infections. *Bioconjugate Chem.* **2015**, *26* (5), 839-849.
21. W. Branderhorst; B. Vastenhouw; F. J. Beekman, Pixel-based subsets for rapid multipinhole SPECT reconstruction. *Phys. Med. Biol.* **2010**, *55* (7), 2023-34.
22. M. N. van Oosterom; R. Kreuger; T. Buckle, et al., U-SPECT-BioFluo: an integrated radionuclide, bioluminescence, and fluorescence imaging platform. *EJNMMI Res.* **2014**, *4* (1), 56-56.
23. A. M. Loening; S. S. Gambhir, AMIDE: a free software tool for multimodality medical image analysis. *Mol. Imaging* **2003**, *2* (3), 131-7.
24. H. Kasuya; D. K. Kuruppu; J. M. Donahue, et al., Mouse models of subcutaneous spleen reservoir for multiple portal venous injections to treat liver malignancies. *Cancer. Res.* **2005**, *65* (9), 3823-7.
25. M. R. Eftink; M. L. Andy; K. Bystrom, et al., Cyclodextrin Inclusion Complexes: Studies of the Variation in the Size of Alicyclic Guests. *Journal of the American Chemical Society* **1989**, *111* (17), 6765-6772.

26. A. Mulder; T. Auletta; A. Sartori, et al., Divalent binding of a Bis(adamantyl)-functionalized calix[4]arene to cyclodextrin-based hosts: An Experimental and Theoretical Study on Multivalent Binding in Solution and at Self-Assembled Monolayers. *Journal of the American Chemical Society* **2004**, 126 (21), 6627-6636.
27. R. Chandra; J. Shamoun; P. Braunstein, et al., Clinical Evaluation of an Instant Kit for Preparation of ^{99m}Tc-MAA for Lung Scanning. *Journal of nuclear medicine : official publication, Society of Nuclear Medicine* **1973**, 14, 702-705.
28. H. Kasuya; D. K. Kuruppu; J. M. Donahue, et al., Mouse Models of Subcutaneous Spleen Reservoir for Multiple Portal Venous Injections to Treat Liver Malignancies. *Cancer Res* **2005**, 65 (9), 3823-3827.
29. R. S. Irwin; P. W. Doherty; T. Bartter, et al., Evaluation of Technetium Pertechnetate as a Radionuclide Marker of Pulmonary Aspiration of Gastric Contents in Rabbits. *Chest* **1988**, 93 (6), 1270-1275.
30. K. M. Tsoi; S. A. MacParland; X. Z. Ma, et al., Mechanism of hard-nanomaterial clearance by the liver. *Nature materials* **2016**, 15 (11), 1212-1221.
31. O. R. Brouwer; N. S. van den Berg; H. M. Matheron, et al., A hybrid radioactive and fluorescent tracer for sentinel node biopsy in penile carcinoma as a potential replacement for blue dye. *European urology* **2014**, 65 (3), 600-9.
32. N. S. van den Berg; O. R. Brouwer; B. E. Schaafsma, et al., Multimodal Surgical Guidance during Sentinel Node Biopsy for Melanoma: Combined Gamma Tracing and Fluorescence Imaging of the Sentinel Node through Use of the Hybrid Tracer Indocyanine Green-^{99m}Tc-Nanocolloid. *Radiology* **2015**, 275, 521-529.
33. G. H. Kleinjan; O. R. Brouwer; H. M. Matheron, et al., Hybrid radioguided occult lesion localization (hybrid ROLL) of (18)F-FDG-avid lesions using the hybrid tracer indocyanine green-(^{99m}Tc)-nanocolloid. *Revista espanola de medicina nuclear e imagen molecular* **2016**, 35 (5), 292-7.





SUPPORTING INFORMATION CHAPTER 3

**A Supramolecular Approach for
Liver Radioembolization**

EXPERIMENTAL SECTION

Stability of $^{99m}\text{Tc-Cy5}_{0.5}\text{CD}_{10}\text{PIBMA}_{39}$ in FCS

$^{99m}\text{Tc-Cy5}_{0.5}\text{CD}_{10}\text{PIBMA}_{39}$ was dissolved in FCS (2.5 $\mu\text{g}/\text{mL}$) and shaken in a water bath at 37 $^{\circ}\text{C}$ for 44 h. After 2, 20, and 44 h 0.1 mL samples were taken and their composition was analyzed by PD-10-SEC.

Stability of $^{99m}\text{Tc-Maa-Ad}$ in FCS

Lyophilized MAA (2 mg) was dissolved in 1 mL of saline (0.9% NaCl, sterile and pyrogen-free, B. Braun Medical Supplies, Inc., Oss, The Netherlands). To one portion 100 mL of a freshly eluted $^{99m}\text{Tc-Na-pertechnetate}$ solution (500 MBq/mL, Mallinckrodt Medical B.V.) was added and the mixture was gently stirred in a shaking water bath for 1 h at 37 $^{\circ}\text{C}$. Thereafter, the solution was washed 2 times PBS by 2 centrifugation steps (3 min, 1,200 rpm). Next, 20 mL of Ad-TFP (10 mg/mL DMSO) was added. After allowing it to react in a shaking water bath for 1 h at 37 $^{\circ}\text{C}$, the reaction mixture was washed 2 times with PBS by 2 centrifugation steps (3 min, 1,200 rpm) and the pellet was dissolved in 1 mL PBS. Of this solution, 0.1 mL was added to 0.9 mL of FCS and was shaken in a water bath at 37 $^{\circ}\text{C}$ up to 44 h. At 2, 20, and 44 h after incubation 0.1 mL samples were taken and their composition analysed by PD-10 SEC.

Stability of $\text{Cy5}_{0.5}\text{CD}_{10}\text{PIBMA}_{39}$ and MAA-Ad complexes in FCS

Mixtures of either MAA-Ad (0.2 mg/mL) with $^{99m}\text{Tc-Cy5}_{0.5}\text{CD}_{10}\text{PIBMA}_{39}$ (10 $\mu\text{g}/\text{mL}$, 1 MBq) or $^{99m}\text{Tc-MAA-Ad}$ (0.2 mg/mL, 1 MBq) with $\text{Cy5}_{0.5}\text{CD}_{10}\text{PIBMA}_{39}$ (10 $\mu\text{g}/\text{mL}$) were prepared in 0.2 mL PBS and the solutions were incubated for 1 h in a shaking water bath at 37 $^{\circ}\text{C}$. Thereafter, the formed complexes were washed twice with PBS by centrifugation (5 min, 3,000 g) and resuspended in 0.2 mL PBS. Subsequently, 0.1 mL thereof was mixed with 1 mL FCS and shaken at 37 $^{\circ}\text{C}$ in a shaking water bath up to 44 h. At 2, 20, and 44 h after incubation 0.1 mL samples were taken and diluted in 1 mL of PBS and after spinning for 5 min at 7,000 rpm, the decay corrected radioactivity of the pellet and supernatant was measured in a dose-calibrator. Hereby a reduction, in the radioactivity of the pellet represents dissociation or instability (% of binding).

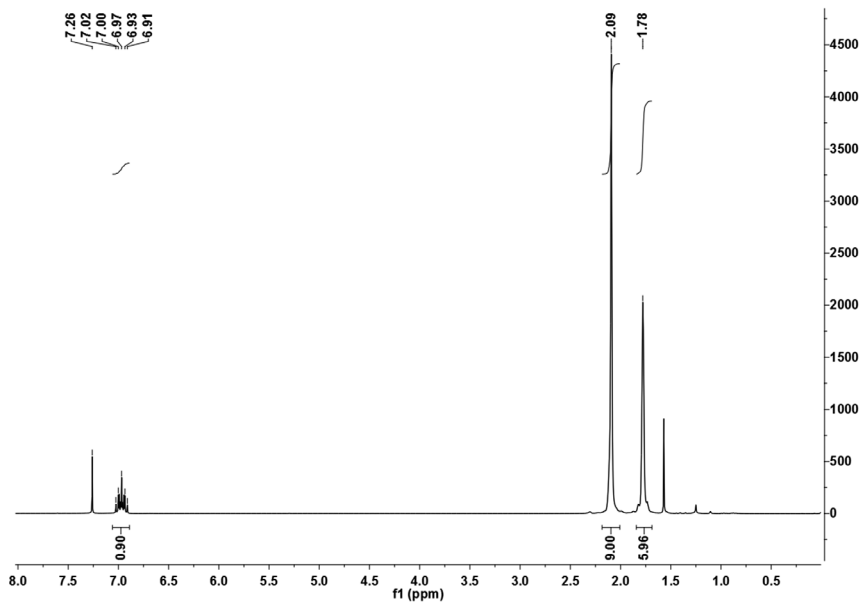
RESULTS AND DISCUSSION

To quantify the difference of $^{99m}\text{Tc-Cy5}_{0.5}\text{CD}_{10}\text{PIBMA}_{39}$ accumulation after pre-administration of nothing, MAA or MAA-Ad for all the investigated organs (Table 1 and Table S1), the relative increase of $^{99m}\text{Tc-Cy5}_{0.5}\text{CD}_{10}\text{PIBMA}_{39}$ accumulation with regard to the $^{99m}\text{Tc-Cy5}_{0.5}\text{CD}_{10}\text{PIBMA}_{39}$ reference distribution (Figure 3) was calculated (Figure S2). If there was a significant increase with $p < 0.01$ this was indicated with a *. When MAA or MAA-Ad was administered i.v. the uptake in the lungs was found highest (but this difference was not significant due to large variations). While locally administered MAA or MAA-Ad resulted in significant increases in spleen, liver and kidneys; pre-administration of MAA or MAA-Ad was performed via the spleen. With the i.v. pre-administration method (Model I) the polymer accumulation increased in more organs compared to the local pre-administration method (Model II), underlining once more the fact that the system works best for the clinically more relevant model i.e. local administration. The significance data can be slightly misleading since increases from e.g. 0.1 %ID/g to 0.3 %ID/g in the brain will be displayed as significant (Table 1 and Table S1).

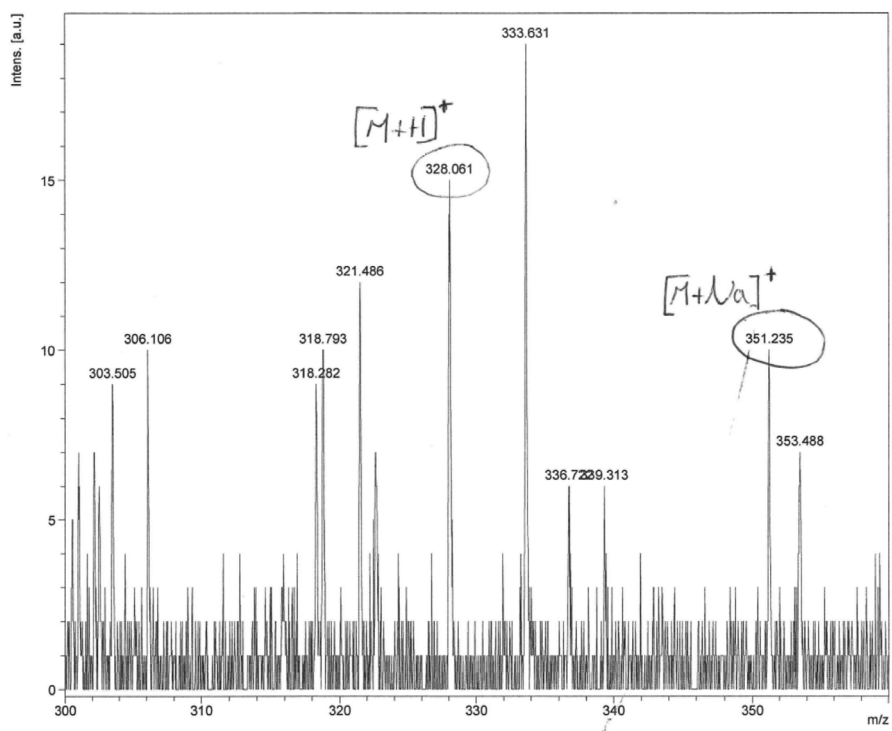
Table S1. The biodistribution of $^{99m}\text{Tc-Cy5}_{0.5}\text{CD}_{10}\text{PIBMA}_{39}$ following injection of: none (reference distribution), MAA, or MAA-Ad and the biodistribution of $^{99m}\text{Tc-MAA-Ad}$ administered via Models I and II. Data (expressed as the mean \pm SD of the percentage of the injected dose per gram tissue (%ID/g) of 5 observations) are calculated from radioactivity counts in various tissues at 2 h post-injection of the tracer.

Tissue	Reference distribution host	Distribution of host ($^{99m}\text{Tc-Cy5}_{0.5}\text{CD}_{10}\text{PIBMA}_{39}$) following injection of indicated guest				Reference distribution guest	
	$^{99m}\text{Tc-Cy5}_{0.5}\text{CD}_{10}\text{PIBMA}$	Model I: MAA	Model I: MAA-Ad	Model II: MAA	Model II: MAA-Ad	Model I: $^{99m}\text{Tc-MAA-Ad}$	Model II: $^{99m}\text{Tc-MAA-Ad}$
	mean	Mean	Mean	Mean	mean	mean	mean
Salivary gland	3.5 \pm 0.4	9.1 \pm 3.3	17.3 \pm 3.5	3.0 \pm 0.6	3.9 \pm 0.1	N.A.	8.9 \pm 1.9
Stomach	4.4 \pm 0.8	19.8 \pm 7.6	10.8 \pm 1.4	3.0 \pm 0.6	2.3 \pm 0.8	11.5 \pm 9.1	12.7 \pm 3.1
Intestines	0.8 \pm 0.3	1.5 \pm 0.6	1.5 \pm 0.3	0.9 \pm 0.0	0.7 \pm 0.3	0.6 \pm 0.3	1.8 \pm 0.5

A



B



◀ **Figure S1. A)** NMR of Ad-TFP measured in CDCl_3 . **B)** Mass spectra of Ad-TFP, only low signals could be obtained as the compound is hard to ionize. Signals corresponding to the mass matrix are therefore clearly visible as well.

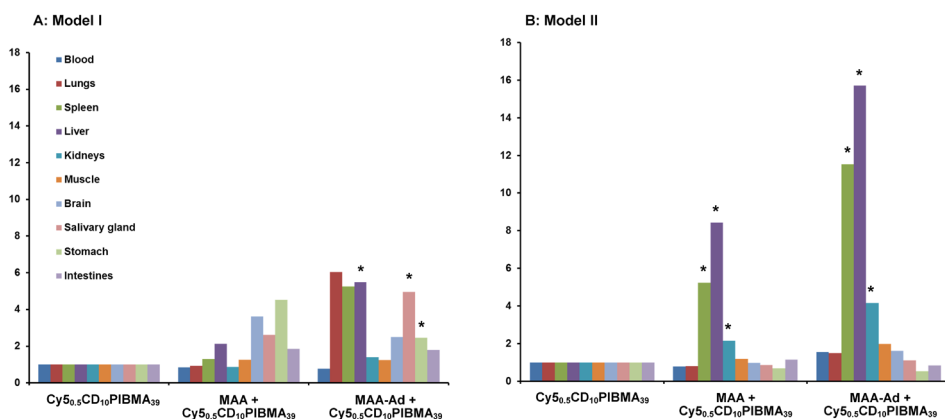


Figure S2. Relative increase of $^{99\text{m}}\text{Tc-Cy5.5CD}_{10}\text{PIBMA}_{39}$ after i.v. (A) or Local (B) administration of MAA or MAA-Ad with respect to $^{99\text{m}}\text{Tc-Cy5.5CD}_{10}\text{PIBMA}_{39}$ accumulation in the indicated organ when no particles are pre-administered. With significance of difference ($p < 0.01$) indicated by *.

Both the individual components and the complexes formed demonstrated a high serum stability (Figure S3). No clear metabolites of the individual components could be defined. This said some dissociation of $^{99\text{m}}\text{Tc}$ was observed both from the individual components as from the complexes formed. Nevertheless, the complex yielded around a 80% stability at 44 h.

As the $\text{Cy5.5CD}_{10}\text{PIBMA}_{39}$ polymer was not optimized for $^{99\text{m}}\text{Tc}$ chelation, but merely provided coordination sides by its free $-\text{COOH}$ moieties, some dissociation of $^{99\text{m}}\text{Tc}$ was observed *in vivo* (Table S1, Figure S3). When this occurred, characteristic uptake in the salivary glands and stomach could be observed. As these findings did not complicate the assessment of the pre-targeting ability, no attempts were made to optimize the chelation stability.

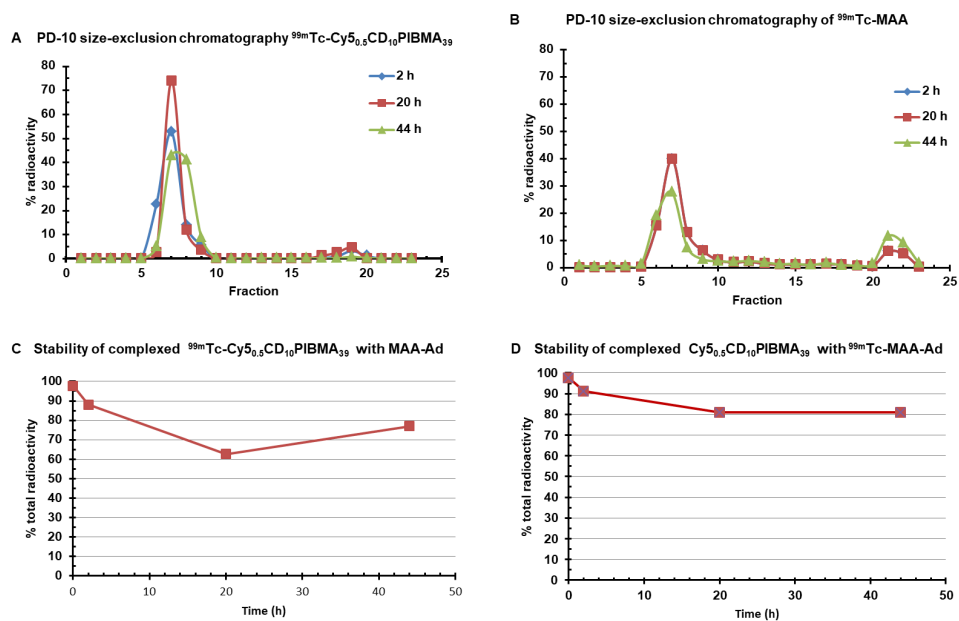


Figure S3. A) Serum stability of $^{99m}\text{Tc-Cy5}_{0.5}\text{CD}_{10}\text{PIBMA}_{39}$ (peak around fraction 18 indicated smaller fragments), **B)** Serum stability of $^{99m}\text{Tc-MAA}$ (peak around fraction 22 indicated some free ^{99m}Tc), **C)** Serum stability of [$^{99m}\text{Tc-Cy5}_{0.5}\text{CD}_{10}\text{PIBMA}_{39}$ * MAA-Ad] complexes, **D)** Serum stability of [$\text{Cy5}_{0.5}\text{CD}_{10}\text{PIBMA}_{39}$ * $^{99m}\text{Tc-MAA-Ad}$] complexes.





Adapted from: Welling MM, Spa SJ, van Willigen DM, Rietbergen DDD, Roestenberg M, Buckle T, van Leeuwen FWB.

J Control Release. 2019;293:126-134